








# Structural Stability of *Pseudomonas aeruginosa* Proteins Associated with the Mucoïd Phenotype: Biomedical Interest in Cystic Fibrosis

Luis Moncayo Molina <sup>1</sup>, Erica Paola Rojas Verdugo <sup>1</sup>, María Agusta Luzuriaga Calle <sup>1</sup>, Aleivi Pérez <sup>2</sup>, María Laura Hurtado-León <sup>3</sup>, Carla Lossada <sup>4</sup>, Lenin González-Paz <sup>4,\*</sup>

<sup>1</sup> Catholic University of Cuenca, Ecuador; lmoncayom@ucacue.edu.ec, (L.M.M.); eprojasv@ucacue.edu.ec, (E.P.R.V.); maria.luzuriaga@ucacue.edu.ec (M.A.L.C.);

<sup>2</sup> University of Zulia. Experimental Faculty of Sciences. General Microbiology Laboratory. Maracaibo-Zulia, Bolivarian Republic of Venezuela; aleviciencias@gmail.com (A.P.);

<sup>3</sup> University of Zulia. Experimental Faculty of Sciences. Maracaibo-Zulia, Bolivarian Republic of Venezuela; marialahurtado@gmail.com (M.L.H.L.);

<sup>4</sup> Venezuelan Institute for Scientific Research (IVIC). Center for Molecular Biomedicine (CBM). Biocomputation Laboratory (LB). Maracaibo-Zulia, Bolivarian Republic of Venezuela; lossadacarla@gmail.com (C.L.); lgonzalezpaz@gmail.com (L.G.P.);

\* Correspondence: lgonzalezpaz@gmail.com (L.G.P.);

Scopus Author ID 6602882448

Received: 9.05.2023; Accepted: 11.08.2023; Published: 4.02.2024

**Abstract:** *Pseudomonas aeruginosa* is a clinically important pathogen resistant to multiple antibiotics and has various virulence factors, such as the production of mucous exopolysaccharides (EPS). The prevalence of chronic infections caused by *P. aeruginosa* is associated with EPS biofilms. Several proteins related to EPS biosynthesis in *P. aeruginosa* have been described. On the other hand, it has been noted that stability and rigidity in certain protein regions are quasi-conserved characteristics that are determinants of biological activity. In this regard, the aim was to describe the intrinsic deformability of various proteins associated with EPS formation in *P. aeruginosa*, using different computational tools that provide information on protein systems' local and global flexibility and rigidity. All the proteins selected in this study, related to the mucoïd phenotype in *P. aeruginosa*, are relatively stable, with similar flexibility among them, as evidenced by both classical and coarse-grained dynamics. It was also observed that protein systems with a tendency towards flexibility are more flexible in a dynamic environment with explicit solvent over time. It was possible to describe the dynamic behavior of proteins associated with the pathogenicity and virulence of *P. aeruginosa*, and it is expected that these approaches will stimulate other theoretical and experimental efforts to consider some of the systems described here as therapeutic targets.

**Keywords:** elastic network models; mucoïd phenotype; molecular dynamics.

© 2024 by the authors. This article is an open-access article distributed under the terms and conditions of the Creative Commons Attribution (CC BY) license (<https://creativecommons.org/licenses/by/4.0/>).

## 1. Introduction

Studying proteins' intrinsic stability or deformability is important because it allows for an indirect description of their structural and conformational stability and the flexibility and rigidity of the different regions or domains that make up a protein system. Therefore, knowing the parameters associated with the deformability of a protein is key for the research and development of drugs and biopharmaceuticals aimed at perturbing the intrinsic stability of a protein of interest associated with disease [1]. There are various computational tools that allow

for the study of both the flexibility and structural and conformational rigidity of various protein systems [2]. In addition, several efforts have been made to study the intrinsic deformability of proteins with a biomedical interest applicable to various diseases such as viral infections [3] and cystic fibrosis [4].

However, there are no reports of a comparative analysis on the intrinsic deformability of proteins described in bacterial pathogens such as *Pseudomonas aeruginosa* associated with the mucoid phenotype implicated in lung infections of patients with cystic fibrosis. *P. aeruginosa* is a Gram-negative bacterial pathogen that is currently considered one of the priority bacteria worldwide for research and development of control alternatives, as it is becoming increasingly difficult to treat due to its multi-drug resistance [5].

The multi-drug resistance of *P. aeruginosa* to antibiotics is favored by the biosynthesis of various proteins associated with the production of its mucous exopolysaccharide (EPS), which provides an additional protective barrier against various antibiotic drugs [6]. Thus, any effort to perturb the stability or formation of the bacterial EPS in *P. aeruginosa* would contribute to increasing the activity of antibiotics [7]. Various proteins associated with the formation of EPS in *P. aeruginosa* have been described, so to know the potential drug targets, as well as the effect that these drugs could have on the biological activity of proteins associated with EPS, it is necessary to describe their intrinsic deformability as has been proposed for other drug targets [8]. In this sense, the present study sought to carry out a comparative analysis that would allow for the description of the intrinsic deformability of various proteins of interest associated with the formation of EPS in *P. aeruginosa*, using different computational tools that allow for obtaining information in terms of local and global flexibility and rigidity of protein systems. The study also sought to provide a theoretical description of the protein regions that could be more susceptible to dynamic changes, and that could be useful as targets for the modulation of virulence factors in *P. aeruginosa*, such as EPS formation.

## 2. Materials and Methods

### 2.1. Databases and selection of structures.

40 protein crystallographic structures related directly or indirectly to the mucoid phenotype in *P. aeruginosa* were randomly selected. The selected structures were: mucC (PDB: 1L2Q), mucA (PDB: 6IN9), rsaL (PDB: 5J2Y), AlgP (PDB: 5GAO), rhII-AHLS (PDB: 3P2H), AlgZ (PDB: 1NTH), prpL (PDB: 2A41), mucD (PDB: 3MH6); AlgR (PDB: 6M8O), LasR (PDB: 3IX3), phzA1-B1 (PDB: 3EX9), LasI (PDB: 1RO5), LasB (PDB: 6FZX), mucB (PDB: 3M4W), rhIB (PDB: 2YJV), LasA (PDB: 3IT5), (PDB: 6CZT), phzM (PDB: 2IP2), LecB (PDB: 1OUX), glpT (PDB: 1PW4), glpD (PDB: 2R45), AlgW (PDB: 5JD8), L22 (PDB: 1BXE), L27 (PDB: 1Y76), phzD2 (PDB: 1NF9), OsmE (PDB: 2F37), hcnA (PDB: 2JPP), hcnB-C (PDB: 2MPF), phzS (PDB: 2RGJ), aprIn (PDB: 2RN4), chiC (PDB: 2Y8V), fabH2 (PDB: 3IL3), phzE2 (PDB: 3R77), plcR (PDB: 3V3W), coxB (PDB: 4W9Z), pqsA (PDB: 5OE3), ippC (PDB: 5VBG), phzC2 (PDB: 6BMC) y pqsB-C (PDB: 6ET2). All structures were taken from the RCSB-protein data bank in PDB format (<https://www.rcsb.org/>). The Molegro Molecular package was used as a viewer and for file preparation.

### 2.2. Preparation of structures for deformability analysis.

The structure files were prepared by cleaning the crystals of any ligands, cofactors, co-solutes, water molecules, or any co-crystallization agent present in the PDB file. The structures

were minimized and dynamized for their analysis and as a previous preparation for the structural deformability analysis guided by elastic networks. Specifically, the systems were designed in explicit water conditions, with a density equivalent to the physiological saline solution ( $\approx 0.9\%$  NaCl). The water used was the TIP3P model, with the ions automatically included by the system to neutralize charges. The simulation systems were cubic boxes of 50 Å that contained a copy of the protein structure to be studied and a number of water molecules automatically adjusted by the system. The periodic boundary conditions for the relaxation phase simulation used the Berendsen algorithm to establish constant temperature (300 K) and pressure (1 atm) systems. The minimization conditions were a simulation based on the steepest descent method, followed by the conjugate gradient method, with 10,000 execution steps. The water molecules were treated as rigid bodies during a 2 fs simulation. The Particle Mesh Ewald method (PME) was used to calculate the electrostatic contributions of the system with a 14 Å cutoff and during 1 fs, as well as a 14 Å cutoff for the contribution of Van der Waals interactions. During the balancing phase, the NVT model was used with production dynamics at 300 K for 100 ps. After the NVT cycle, the NPT model was applied to balance the system at constant pressure (1 atm) and temperature (300 K). In parallel, and to compensate for geometric constraints, the SHAKE algorithm was considered applied for 2 fs. For the final production phase, the proposed conditions were the same as the NPT model for sampling the minimum energy structure after 100 ns of simulation. All adjustments and additional molecular dynamics conditions were carried out in the myPresto package [9].

The minimum energy structure was compared with the initial structure in each case to determine the Root Mean Square Deviations (RMSD) using the following equation,

$$RMSD = \sqrt{\frac{1}{n} \sum_{i=1}^n \delta_i^2} \quad (\text{eq.1})$$

where  $\delta_i$  is the distance between atom  $i$  and either a reference structure or the mean position of the  $n$  equivalent atoms. Similarly, to predict the stability of the complexes, the  $R_g$  was calculated using the Hullrad tools ([http://52.14.70.9/index\\_test.html](http://52.14.70.9/index_test.html)) [10] and the scfbio supercomputing service (<http://www.scfbio-iitd.res.in/software/proteomics/rgnew.jsp>).

### 2.3. Comparative analysis of structural stability using elastic network models.

In this study, elastic network models (ENM) were considered because they allow the study of conformational changes in terms of stiffness or flexibility of protein systems and offer structural configurations or low-frequency modes that have been shown to be similar to the minimum energy structures obtained through classical dynamics, but with a lower computational cost. ENMs use normal mode analysis (NMA) models based on the study of coarse-grained networks, which means that they typically only consider  $C\alpha$  atoms to describe the vibrational dynamics of protein systems around a minimum energy configuration. Based on this, the goal was to calculate the RMSD using the elastic network tools webNMA (<http://apps.cbu.uib.no/webnma3>) and NMSim (<https://cpclab.uni-duesseldorf.de/nmsim/>). To learn more about the details of the elastic network models applied in this study, we suggest reviewing [11,12].

### 2.4. Analysis of quasi-rigid domains with SPECTRUS and structural energy frustration.

To predict changes in the flexible regions of the protein systems considered, the SPECTRUS server (<http://spectrus.sissa.it/>) was used, which allows for a decomposition of the

number of quasi-rigid domains (Q) of protein complexes through the analysis of the fluctuation of the distance between interacting amino acid pairs, as well as the prediction of a quality score (QS) associated with the prediction of structural flexibility or stiffness. Variations in the number of Q represent modifications in the number of domains of the structure, while an increase or decrease in the QS value represents an increase or decrease, respectively, in the accuracy of the prediction of the stiffness of the systems [13]. In addition, the Frustratometer software (<http://frustratometer.qb.fcen.uba.ar/>) was used, which is an algorithm inspired by the energy landscape theory that aims to quantify the degree of local frustration manifested in protein molecules through their conformational perturbations [14].

### 3. Results and Discussion

Table 1 shows the dynamic parameters of each minimum energy structure considered in this study in terms of RMSD and Rg after 100 ns of MD. The structures presented an average in terms of RMSD =  $2.61 \pm 0.86 \text{ \AA}$ , with maximum values of RMSD =  $5.34 \text{ \AA}$  for structures such as hcnA (PDB: 2JPP) and a minimum of RMSD =  $1.12 \text{ \AA}$  for structures such as LasA (PDB: 3IT5). Despite the fact that a similar fluctuation of RMSD values was predicted between the initial structures and those of minimum energy, this was statistically differential ( $t = -10.32$ ,  $df = 38$ ,  $p < 0.0001$ ,  $\alpha = 0.01$ ). The low fluctuation presented between the initial structures and those of minimum energy (with a difference of  $\approx 0.08 \text{ \AA}$ ) is associated with stable structures throughout the considered simulation time.

In relation to the fluctuation of the radius of the structures, an  $R_g = 17.12 \pm 3.66 \text{ \AA}$  and an  $R_g = 17.39 \pm 3.61 \text{ \AA}$  were predicted, according to the Hullrad and scfbio methods, respectively. Despite the similarity between the Rg values obtained by the methods used, the differences between the predicted values after the simulation at 100 ns were statistically significant for both Hullrad with an  $R_g = 16.86 \pm 3.56 \text{ \AA}$  ( $t = 2.88$ ,  $df = 38$ ,  $p = 0.003$ ,  $\alpha = 0.01$ ) and for scfbio with an  $R_g = 16.55 \pm 3.10 \text{ \AA}$  ( $t = 3.32$ ,  $df = 38$ ,  $p = 0.0009$ ,  $\alpha = 0.01$ ), as observed in terms of RMSD. After 100 ns of MD, minimum values for hullraid and india of  $R_g = 10.82 \text{ \AA}$  (OsmE, PDB: 2F37) and  $R_g = 11.12 \text{ \AA}$  (rsaL, PDB: 5J2Y), respectively, as well as a maximum value of  $R_g = 22.80 \text{ \AA}$  for both methods in structures such as glpT (PDB: 1PW4) and glpD (PDB: 2R45), respectively (Table 1). The overall results of RMSD and Rg show that the structures considered are stable after the MD simulation at 100 ns.

**Table 1.** RMSD and Rg parameters obtained via MD from protein structures related to the mucoid phenotype in

*Pseudomonas aeruginosa.*

Name	PDB	RMSD <sup>a</sup>	RMSD <sup>b</sup>	Rg1 <sup>a</sup>	Rg1 <sup>b</sup>	Rg2 <sup>a</sup>	Rg2 <sup>b</sup>
AlgF	6CZT	2.45	2.50	12.18	12.39	12.27	12.41
AlgP	5GAO	2.68	2.81	18.25	18.27	20.60	20.48
AlgR	6M8O	2.33	2.44	13.09	13.43	13.40	13.56
AlgW	5JD8	2.19	2.24	21.86	21.18	21.95	17.68
AlgZ	1NTH	1.87	1.94	21.17	21.46	21.31	22.53
aprIn	2RN4	3.23	3.37	13.63	13.01	13.67	12.99
chiC	2Y8V	2.37	2.44	19.37	19.14	19.52	19.21
coxB	4W9Z	2.32	2.44	14.32	14.24	14.39	14.25
fabH2	3IL3	3.50	3.57	17.97	17.27	16.86	16.00
glpD	2R45	1.73	1.79	22.75	22.79	22.80	22.80
glpT	1PW4	3.09	3.17	23.33	22.80	23.41	19.95
hcnA	2JPP	5.32	5.34	13.17	11.27	13.21	13.21
hcnB-C	2MPF	3.70	3.77	15.34	14.97	15.37	14.96
ippC	5VBG	2.25	2.39	14.01	13.81	14.22	13.97
L22	1BXE	4.03	4.00	12.35	11.78	12.67	11.98
L27	1Y76	3.18	3.22	14.63	14.32	14.67	14.32
LasA	3IT5	1.07	1.12	14.95	15.07	15.07	15.10

Name	PDB	RMSD <sup>a</sup>	RMSD <sup>b</sup>	Rg1 <sup>a</sup>	Rg1 <sup>b</sup>	Rg2 <sup>a</sup>	Rg2 <sup>b</sup>
LasB	6FZX	1.31	1.39	18.68	18.69	18.79	18.73
LasI	1RO5	1.94	2.03	16.15	16.03	16.25	16.07
LasR	3IX3	1.91	1.96	15.38	15.21	15.43	15.22
LecB	1OUX	1.66	1.79	13.46	13.78	13.66	13.83
mucA	6IN9	2.37	2.44	20.55	19.92	21.76	20.15
mucB	3M4W	2.38	2.47	20.28	19.82	20.33	18.11
mucC	1L2Q	3.78	3.82	22.43	20.72	22.67	20.92
mucD	3MH6	2.70	2.80	23.05	21.78	23.15	16.67
OsmE	2F37	3.90	3.98	10.52	10.82	12.75	12.94
phzA1-B1	3EX9	2.89	2.89	16.69	17.07	16.87	17.06
phzC2	6BMC	2.04	2.28	19.46	19.80	19.83	19.35
phzD2	1NF9	1.30	1.40	16.01	16.06	16.16	16.14
phzE2	3R77	1.50	1.60	15.53	15.98	15.92	16.22
phzM	2IP2	2.80	2.89	22.15	21.38	22.29	21.41
phzS	2RGJ	3.56	3.63	17.46	15.95	17.74	16.20
plcR	3V3W	1.80	1.83	20.92	20.76	20.98	20.43
pqsA	5OE3	2.02	2.07	20.83	20.88	20.88	15.62
pqsB-C	6ET2	2.09	2.12	20.15	20.28	20.32	20.31
prpL	2A41	2.39	2.50	14.69	14.02	15.28	14.54
rhlB	2YJV	3.11	3.24	14.44	14.84	14.60	14.92
rhlI-AHLS	3P2H	1.99	2.06	15.64	15.49	15.86	14.41
rsaL	5J2Y	2.18	2.21	11.21	11.13	11.43	11.12

PDB, protein data bank; RMSD, root mean square deviation; <sup>a</sup>, values calculated from the crystal; <sup>b</sup>, values calculated at 100 ns of MD; Rg1, hullrad ([http://52.14.70.9/index\\_test.html](http://52.14.70.9/index_test.html)); Rg2, scfbio (<http://www.scfbio-iitd.res.in/software/proteomics/rgnew.jsp>).

### 3.1. Analysis of dynamic parameters obtained via ENM from protein structures related to the mucoid phenotype in *P. aeruginosa*.

In terms of coarse-grained RMSD guided by ENM, an initial average of  $3.98 \pm 2.00 \text{ \AA}$  was predicted, with maximum values of  $\text{RMSD} = 8.44 \text{ \AA}$  for structures such as phzA1-B1 (PDB: 3EX9) and a minimum of  $\text{RMSD} = 1.60 \text{ \AA}$  for structures such as rhlB (PDB: 2YJV). As for the minimum energy structures at the end of the simulation, an average of  $3.47 \pm 1.74 \text{ \AA}$  was predicted, with maximum values of  $\text{RMSD} = 8.23 \text{ \AA}$  for structures such as L27 (PDB: 1Y76) and a minimum of  $\text{RMSD} = 1.68 \text{ \AA}$  for structures such as AlgR (PDB: 6M8O) and coxB (PDB: 4W9Z) (see Table 2). It is important to note that the structures predicted via ENM with minimum and maximum fluctuations differ from those observed with minimum and maximum values obtained by MD. In this sense, and as with MD, when comparing the initial structures with the final conformations offered by ENM, it was found that although the difference in terms of RMSD fluctuation was only  $\approx 0.50 \text{ \AA}$  (characteristic of stable structures), the average of the trajectories was significantly different ( $t = 3.31$ ,  $df = 38$ ,  $p = 0.0009$ ,  $\alpha = 0.01$ ) (Table 2).

On the other hand, the RMSF values calculated using ENM showed an initial average of  $2.08 \pm 0.52 \text{ \AA}$ , with minimum fluctuation values ( $\text{RMSF} = 0.98 \text{ \AA}$ ) and maximum ( $\text{RMSF} = 3.43 \text{ \AA}$ ) for the pqsA structures (PDB: 5OE3) and OsmE (PDB: 2F37), respectively. In addition, no significant difference ( $t = 1.24$ ,  $df = 38$ ,  $p = 0.11$ ,  $\alpha = 0.01$ ) was predicted regarding RMSF between the crystal structure (initial) and the minimum energy structure calculated using ENM. The structures that presented minimum and maximum values after the ENM simulation were plcR (PDB: 3V3W) and L27 (PDB: 1Y76) with an  $\text{RMSF} = 1.08 \text{ \AA}$  and  $\text{RMSF} = 3.37 \text{ \AA}$ , respectively (Table 2).

It is important to note that after the tests with structures simulated at 100 ns of MD and then analyzed using ENM, one of the few structures, such as L27 (PDB: 1Y76) (Figure 1A), maintained the highest predicted fluctuation in both in terms of RMSD and RMSF, indicative of a highly flexible protein system.

When comparing the average of the trajectories generated under the conditions of this study for the structures in terms of RMSD using MD and ENM, significant differences were observed between both methods ( $t = 2.75$ ,  $df = 76$ ,  $p = 0.003$ ,  $\alpha = 0.01$ ), which could be associated with the high fluctuation of the presented structures or with the inherent differences of each method [15]. However, it is important to mention that the absence of similarity between both methods may be due to the fact that the ENM approach offered structures with a lower fluctuation in terms of RMSD compared to the values calculated by MD (Table 1; Table 2). Specifically,  $\approx 15\%$  of the minimum energy structures obtained via MD presented atypical values  $\approx 4 \text{ \AA}$  in relation to the average, compared to  $\approx 2\%$  of the structures obtained through ENM deviated from their average with even lower values ( $\approx 2 \text{ \AA}$ ). Therefore, while it is suggested to carry out comparative analyses when using both minimization methods, especially since our overall results differ from those reported [15], the ability of the ENM approach to generate very stable structures at the level of structural flexibility and comparable to those obtained by MD as has been reported [16-19] should be highlighted.

The results obtained using the dynamic methods of MD and ENM in terms of RMSD, RMSF, and Rg allow us to infer globally that the protein structures considered in this study for being related to the mucoid phenotype in *P. aeruginosa* present a similar behavior in terms of stability according to the methods considered. Additionally, the stability of the proteins of interest was calculated by predicting the fluctuation of the number of quasi-rigid domains (Q) of the structures and by comparing the quality score (QS) associated with the accuracy of the prediction of structural flexibility or rigidity.

The global average of the number of quasi-rigid domains after the simulation guided by SPECTRUS and from the minimum energy structures obtained by MD was  $Q = 5.74 \pm 2.65$ , a value similar to that predicted for the average of the starting or crystallographic structures ( $Q = 5.58 \pm 2.89$ ). These results associated with the quasi-rigidity measured in terms of Q show a non-significant fluctuation of the rigid regions of the structures ( $t = -0.24$ ,  $df = 76$ ,  $p = 0.40$ ), indicative of stable protein systems. Similarly, no difference was found in the number or total regions of predicted quasi-rigid domains ( $t = -0.66$ ,  $df = 76$ ,  $p = 0.25$ ), and no difference in the quality in terms of QS of the stiffness models of the minimum energy structures for the maximum values ( $t = 0.88$ ,  $df = 37$ ,  $p = 0.19$ ,  $\alpha = 0.01$ ) and the minimum fluctuation values ( $t = 1.86$ ,  $df = 37$ ,  $p = 0.03$ ,  $\alpha = 0.01$ ). Specifically, the average after the simulation was  $QS = 3.90 \pm 3.64$ , with minimum values of  $QS = 2.23$  and maximum values of  $QS = 24.90$  for structures such as LasA (PDB: 3IT5) and AlgW (PDB: 5JD8), respectively. The QS values after the simulation differ from the values obtained from the starting or crystallographic structures, with a  $QS \approx 5.56$ , with minimum values of  $QS = 2.17$ , and maximum values of  $QS = 43.54$  for structures such as phzE2 (PDB: 3R77) and AlgW (PDB: 5JD8), respectively.

These predictions in terms of QS allow us to infer that despite the few differences in the RMSD, RMSF, and Rg parameters calculated via MD and ENM, the distributions of the flexible regions of the structures studied show protein systems with a tendency towards flexibility or rather, to be more flexible in a dynamic environment with explicit solvent. The predictions made in this study show that the proteins considered associated with the mucoid phenotype in *P. aeruginosa* present stable conformations but with a tendency towards relaxation or flexibility in dynamic environments over time. Knowing the dynamic aspect of this group of proteins is important because they could be considered as targets or candidates for therapeutic targets of drugs that can alter their structural flexibility to modulate mucopolysaccharide production, as has been suggested [20-22].

**Table 2.** Dynamic parameters obtained via ENM from protein structures related to the mucoid phenotype in *Pseudomonas aeruginosa*.

Name	PDB	RMSD <sup>a</sup>	RMSD <sup>b</sup>	RMSF <sup>a</sup>	RMSF <sup>b</sup>	Q <sup>a</sup>	Q <sup>Sa</sup>	Q <sup>b</sup>	Q <sup>Sb</sup>
AlgF	6CZT	2.52	3.02	1.94	2.75	3	3.52	6	2.37
AlgR	6M8O	2.70	1.68	1.70	1.19	9	2.78	7	2.72
AlgW	5JD8	5.88	5.05	2.17	2.26	2	43.54	2	24.90
LecB	1OUX	1.92	2.27	1.60	2.01	3	3.32	2	3.55
LasA	3IT5	1.66	2.00	2.09	1.69	10	2.46	10	2.23
LasB	6FZX	2.31	2.49	1.47	1.91	2	4.01	2	3.83
LasI	1RO5	3.06	3.05	1.81	1.80	2	3.73	6	2.92
LasR	3IX3	3.02	1.77	1.93	1.78	8	2.70	5	2.88
mucA	6IN9	3.82	4.08	2.13	2.10	3	4.66	3	4.20
mucB	3M4W	4.54	2.13	1.63	1.38	3	5.42	8	3.24
mucC	1L2Q	3.45	3.61	1.98	2.12	2	22.62	2	6.25
mucD	3MH6	3.53	3.09	1.81	1.69	3	8.01	3	4.95
rhlI-AHLS	3P2H	2.75	2.15	2.02	2.24	7	3.42	6	3.36
rsaL	5J2Y	4.24	2.53	2.39	1.67	6	4.35	6	3.38
AlgZ	1NTH	2.00	3.21	1.59	1.79	8	3.08	10	2.48
AlgP	5GAO	5.22	3.75	2.11	1.28	5	3.64	5	3.80
L22	1BXE	4.38	4.09	2.25	2.33	2	4.60	6	2.83
L27	1Y76	8.34	8.23	2.38	3.37	5	3.40	4	3.47
phzD2	1NF9	2.47	1.78	2.55	1.94	7	2.29	8	2.37
glpT	1PW4	4.08	2.70	1.79	1.67	8	3.53	10	3.13
prpL	2A41	7.92	7.08	2.74	2.75	4	3.72	4	4.75
OsmE	2F37	4.45	3.38	3.43	3.24	6	2.59	6	2.34
phzM	2IP2	4.54	3.23	2.07	1.72	4	9.23	7	2.99
hcnA	2JPP	6.10	3.60	2.63	1.96	6	4.38	6	3.88
hcnB-C	2MPF	3.38	3.46	2.54	1.79	3	3.23	3	2.97
glpD	2R45	2.97	2.99	1.56	1.56	3	4.85	3	3.63
phzS	2RGJ	7.90	6.94	3.09	3.01	3	5.70	6	3.67
aprIn	2RN4	4.54	2.41	1.73	1.22	10	2.73	5	3.00
chiC	2Y8V	6.18	3.61	2.34	1.82	2	4.20	4	2.54
rhlB	2YJV	1.60	2.64	2.24	2.60	10	2.41	8	2.79
phzA1-B1	3EX9	8.44	7.59	3.09	2.68	8	2.35	10	2.77
fabH2	3IL3	8.05	7.85	3.11	2.97	2	17.10	2	8.52
phzE2	3R77	1.74	2.41	2.22	1.55	7	2.17	8	2.45
plcR	3V3W	2.79	2.22	1.52	1.08	10	3.54	10	2.86
coxB	4W9Z	1.61	1.68	1.50	1.85	8	2.82	8	3.25
pqsA	5OE3	2.41	3.40	0.98	1.43	6	2.89	2	2.80
ippC	5VBG	3.04	3.01	1.65	1.83	10	2.57	4	2.90
phzC2	6BMC	2.79	2.41	1.83	1.58	9	3.16	10	2.67
pqsB-C	6ET2	3.01	2.91	1.70	2.28	9	2.33	7	2.54

PDB, protein data bank; RMSD, root mean square deviation; RMSF, root mean square fluctuation; Q, number of domains or quasi-rigid or less flexible (low mobility) regions; QS, quality score for true domains or quasi-rigid or less flexible (low mobility) regions. The higher the score, the more likely the prediction of rigidity; a, values calculated from the crystal; b, values calculated from the minimum energy structure obtained after a coarse-grained simulation of 1,500 conformations.

### 3.2. Analysis of energy frustration of protein structures related to the mucoid phenotype in *P. aeruginosa*.

Energy frustration analysis allowed for predicting the local energy stability of the protein structures of interest. Although no statistical differences were observed in the number or quantity of regions associated with energy fluctuations ( $t = -1.16$ ,  $df = 38$ ,  $p = 0.12$ ,  $\alpha = 0.01$ ), nor in the minimum ( $t = 1.86$ ,  $df = 37$ ,  $p = 0.03$ ,  $\alpha = 0.01$ ) or maximum ( $t = 0.88$ ,  $df = 37$ ,  $p = 0.19$ ,  $\alpha = 0.01$ ) ranges of the concentrations of energetically frustrated residues at the total level, however, it was predicted that  $\approx 60\%$  of the structures presented changes at the level of density or concentration of their local energy stability.

Changes at the level of global energy frustration showed an average of  $\approx 6$  altered regions after MD simulations, with structures with a minimum of 2 altered regions (AlgF, PDB: 6CZT) and a maximum of 11 (glpT, PDB: 1PW4; phzM, PDB: 2IP2; pqsA, PDB: 5OE3)

(Table 3). Specifically,  $\approx 92\%$  of the proteins that showed energetic disturbances at the structural level after MD presented these fluctuations in their central regions, maintaining the initial energetic stability in the lateral regions. The energetic frustration presented by structures such as glpT (Figure 1b) corresponds to its high dynamic fluctuation predicted in terms of Rg (Table 1).

The high variability in deformability presented by this group of proteins, although it shows a heterogeneous behavior with an unclear trend in terms of flexible and rigid regions, allows to discriminate between those proteins with a quasi-rigidity and moderately conserved (or well-defined) energetic frustration from those with greater intrinsic flexibility, key conformational aspects for the selection of candidate targets [23-33].

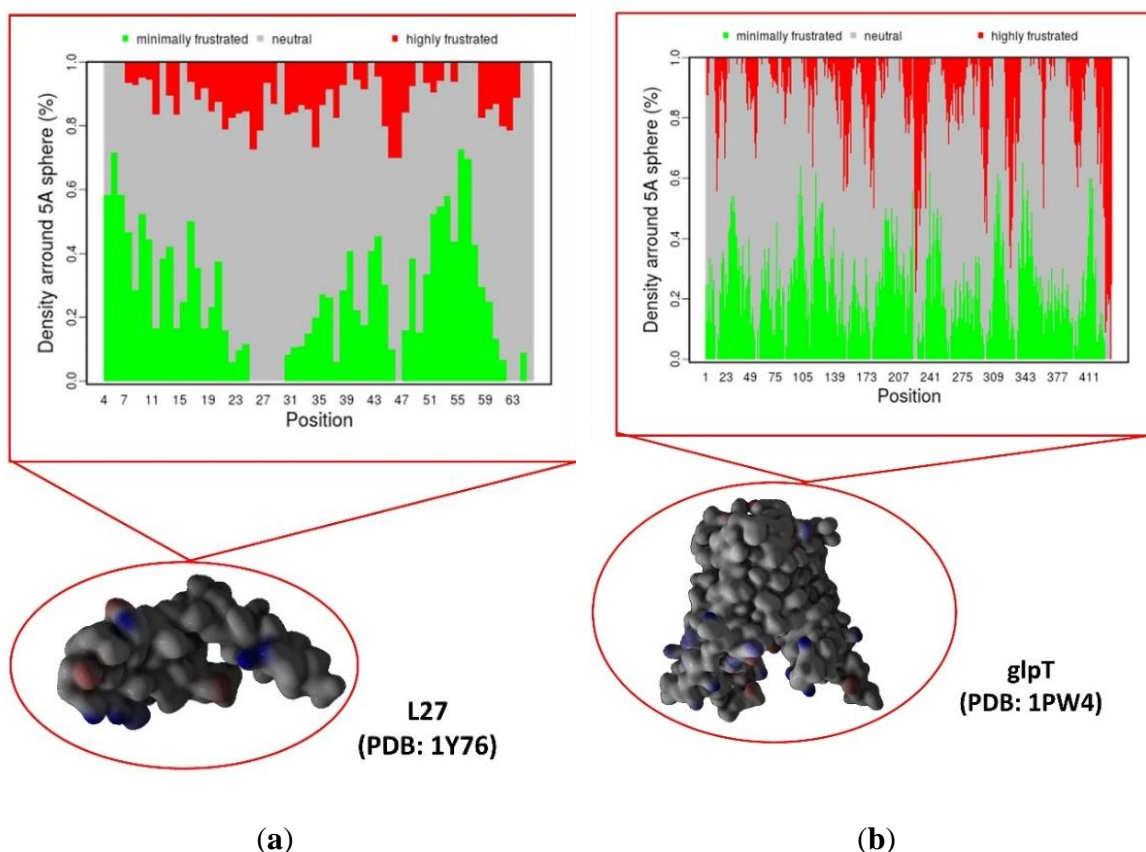


**Figure 1.** Bar diagram of the energetic frustration of two model proteins present in the group of studied proteins. **a)** In the upper panel, the bar diagram of the energetic frustration of protein L27 (PDB: 1Y76) is shown with less observable frustration by the red bars than that presented by **b)** protein glpT (PDB: 1PW4).

**Table 3.** Energetic frustration regions detected in protein structures related to the mucoid phenotype in *Pseudomonas aeruginosa*.

Name	PDB	Frustratometer <sup>a</sup>	Position <sup>a</sup>	Frustratometer <sup>b</sup>	Position <sup>b</sup>
AlgF	6CZT	0.2-0.4	38-63, 68, 73-118	0.2-0.4	38-114, 118
AlgR	6M8O	0.2-0.5	1-33, 40, 47-54, 61-68, 75-82, 89, 96-113	0.2-0.5	1-6, 12, 19-33, 40, 47-82, 89, 96-113
AlgW	5JD8	0.2-0.6	60, 77-134, 155-176, 197, 218, 239, 260, 281, 302	0.1-0.5	15, 32-49, 66-186, 207-228, 249, 270
LecB	1OUX	0.2-0.8	6-68, 75-82, 89-96, 104-113	0.1-0.6	1, 6-19, 26-33, 40-68, 75, 82, 89-96, 104-113
LasA	3IT5	0.2-0.6	1-41, 52-63, 74-109, 123-151, 179	0.2-0.5	1-41, 52-109, 123-151, 165, 179
LasB	6FZX	0.2-0.6	1, 17, 35, 53, 71, 89, 110-179, 202, 225, 248-294	0.2-0.6	1, 17, 35-71, 89, 110-156, 179, 202, 225, 248-271, 294
LasI	1RO5	0.2-0.7	11-47, 59, 71-83, 95, 109, 125-141, 157-173, 189	0.1-0.7	1-11, 23, 35, 47, 59-71, 83, 95, 109, 125-173, 189
LasR	3IX3	0.1-0.7	7-36, 56, 76-86, 96, 108, 121-134, 147-160	0.1-0.7	7, 16, 26-134, 147, 160



Name	PDB	Frustratometer <sup>a</sup>	Position <sup>a</sup>	Frustratometer <sup>b</sup>	Position <sup>b</sup>
mucA	6IN9	0.1-0.6	23, 40, 57, 74, 91, 110-173, 194-215, 236, 257, 278	0.1-0.6	1-32, 49-83, 102-165, 186-207, 228, 249-270
mucB	3M4W	0.2-0.7	25-42, 59-93, 113, 135-179, 201, 223-289	0.1-0.7	1, 16-67, 84, 104, 126-170, 192-280
mucC	1L2Q	0.3-0.7	2-37, 61-85, 111, 127-143, 159, 175, 191	0.2-0.8	2-25, 37, 49, 61-111, 127-159, 175-191
mucD	3MH6	0.2-0.6	11-35, 59, 83-140, 170, 200, 230, 260-350, 380	0.2-0.6	1-45, 69-93, 120, 150, 180-240, 270-330, 360, 390
rhlI-AHLS	3P2H	0.1-0.6	1-9, 19-30, 41-74, 85-154, 169-184	0.2-0.6	1-9, 19-30, 41, 52-124, 139, 154, 169, 184
rsaL	5J2Y	0.2-0.6	13-21, 33-49, 53-61, 69-77	0.1-0.8	13-21, 25-61, 65-77
AlgZ	1NTH	0.1-0.5	2-145, 180, 215-390, 425	0.1-0.5	1-24, 51-109, 144-179, 214-319, 354, 389, 424
AlgP	5GAO	0.1-0.6	2147, 2171, 2195, 2243, 2267-2315, 2339-2363, 2387	0.1-0.6	2147, 2171, 2195, 2219, 2243, 2267-2291, 2315, 2339, 2363-2387
L22	1BXE	0.2-0.7	2-8, 12-24, 28-60	0.2-0.7	2-12, 16, 20-24, 28-32, 36, 40, 44-60, 64
L27	1Y76	0.2-0.7	1, 4-63	0.2-0.7	1, 4-23, 31-43, 47-59, 63
phzD2	1NF9	0.2-0.8	1-77, 90-120, 136, 152-200	0.1-0.8	1, 12-25, 38-120, 136, 152, 168-200
glpT	1PW4	0.2-0.7	5, 27-53, 79-109, 143, 177, 211, 245, 279, 313-381, 415	0.1-0.5	1, 23-49, 75, 105-139, 173, 207, 241, 275, 309, 343-377, 411
prpL	2A41	0.2-0.7	7-21, 31-41, 51-61, 66-71	0.1-0.8	4-7, 11-41, 46, 51-61, 66-71
OsmE	2F37	0.2-0.8	71-89, 92-98, 106-114, 118	0.2-0.7	71-83, 86-98, 102, 106-110, 118
phzM	2IP2	0.1-0.8	5, 22-42, 62, 82-115, 131, 157-183, 209, 235, 261, 287-313	0.2-0.7	22, 42, 62, 82, 105, 131, 157-183, 209, 235, 261, 287-313
hcnA	2JPP	0.3-0.8	1-4, 7-26, 30-38, 42, 46-50	0.2-0.5	1-4, 7-22, 30-38, 42-50
hcnB-C	2MPF	0.2-0.7	534, 556-589, 600-611, 622-644, 655, 666	0.2-0.6	534-589, 600-633, 644-655, 666
glpD	2R45	0.1-0.6	1-81, 113, 149-185, 221-257, 293, 329, 365, 401, 437	0.1-0.7	1-25, 81-113, 149-257, 293, 329-365, 401, 437
phzS	2RGJ	0.2-0.7	4-22, 29-36, 43-57, 64, 71-78, 92-107	0.2-0.9	4-36, 43-57, 64, 71-78, 92, 99-107
aprIn	2RN4	0.2-0.6	2, 12-47, 54-61, 68-104	0.2-0.5	1-6, 12-40, 54, 61-104
chiC	2Y8V	0.2-0.6	8, 23, 40-57, 74, 91, 110, 132-176, 198-264	0.1-0.6	8, 40-57, 74, 91, 110-264
rhlB	2YJV	0.1-0.7	2-47, 57-108, 121-160	0.1-0.8	2-9, 17-47, 57-160
phzA1-B1	3EX9	0.2-0.7	10-55, 64-114, 126-150	0.2-0.6	10-55, 64-114, 126-138, 150
pqsD	3H77	0.1-0.7	6, 19, 33, 40-82, 89-104	0.2-0.7	1, 6-19, 33, 40-82, 89-104
fabH2	3IL3	0.2-0.6	2-78, 91, 105, 121, 137, 153-201	0.2-0.8	2-13, 26-65, 78-91, 105-137, 153, 169, 185-201
phzE2	3R77	0.2-0.7	1-22, 46, 70, 94, 121, 152, 183, 214, 245-338, 369	0.2-0.5	1-22, 46, 70, 94, 121, 152-183, 214, 245-338, 369
plcR	3V3W	0.1-0.6	127-160, 171-226, 237-248, 259	0.2-0.6	127, 138-160, 171-248, 259
coxB	4W9Z	0.2-0.8	2-22, 46-94, 121, 152, 183-214, 245-276, 307, 338, 369	0.2-0.8	1-21, 45-69, 93, 120, 151, 182-213, 244, 275, 306, 337, 368
pqsA	5OE3	0.2-0.6	33-40, 47, 61-122, 131-149	0.2-0.7	33-40, 47, 61-122, 131, 140, 149
ippC	5VBG	0.2-0.8	1-21, 44-116, 145, 174-290, 319-377	0.2-0.7	1-21, 44, 67-232, 261, 290, 319-377
phzC2	6BMC	0.2-0.8	9-141, 168, 195, 222-276	0.2-0.8	9-141, 168, 195, 222-276
pqsB-C	6ET2	0.2-0.4	38-63, 68, 73-118	0.2-0.4	38-114, 118

PDB, Protein Data Bank; Frustratometer, range or region of high configurational energetic frustration (unaffected residues are marked in red); a, values calculated from the crystal; b, values calculated at 100 ns of MD.

In fact, the proteins AlgF (PDB: 6CZT), AlgW (PDB: 5JD8), LasR (PDB: 3IX3), mucA (PDB: 6IN9), mucB (PDB: 3M4W), mucC (PDB: 1L2Q), mucD (PDB: 3MH6), AlgZ (PDB: 1NTH), glpT (PDB: 1PW4), aprIn (PDB: 2RN4), fabH2 (PDB: 3IL3), coxB (PDB: 4W9Z) and pqsB-C (PDB: 6ET2) were the ones that presented the greatest energetic fluctuation at the conformational level (Table 3), so they represent the group of analyzed proteins with the greatest intrinsic flexibility at the energetic level according to the conditions of this study, which would make them candidates for ligands that are capable of inducing changes at the level of their local stabilization.

Finally, the observations obtained in this study constitute a first approach to the intrinsic characteristics of deformability and stability of proteins associated with the production of exopolysaccharide of one of the most relevant clinical pathogens worldwide [34-45], so it seeks to encourage research, development, and reuse of drugs directed at the structures of interest presented here. In this sense, our group is currently working in this direction [46-49].

#### **4. Conclusions**

The proteins selected in this study for being related to the mucoid phenotype in *P. aeruginosa* are relatively stable at the dynamic level over the MD simulation time considered. The results obtained through classical and coarse-grained dynamics methods allow us to infer that under the conditions of this study, the protein structures associated with the virulence of *P. aeruginosa* present similar behaviors in terms of stability. Similarly, it was observed that protein systems with a tendency towards flexibility are more flexible over time in a dynamic environment with explicit solvents. It was observed that models based on ENM can generate very stable structures in terms of structural flexibility and are comparable to those obtained by MD. In this sense, it was possible to describe the dynamic behavior of this group of proteins associated with the pathogenicity and virulence of *P. aeruginosa*. It is expected that these approaches will stimulate other theoretical and experimental efforts to consider some of the systems described here as candidate targets for therapeutic compounds that can alter the production of mucopolysaccharide by this important pathogen.

#### **Funding**

This research received no specific grant from public, commercial, or not-for-profit funding agencies.

#### **Acknowledgments**

This research has no acknowledgment.

#### **Conflicts of Interest**

The authors declare that they have no known competing financial interests or personal relationships that could have appeared to influence the work reported in this paper.

#### **References**

1. Depond, M.; Henry, B.; Buffet, P.; Ndour, P. A. Methods to Investigate the Deformability of RBC During Malaria. *Front Physiol* **2020**, *10*, 1613, <https://doi.org/10.3389/fphys.2019.01613>.

2. Sun, Z.; Liu, Q.; Qu, G.; Feng, Y.; Reetz, M.T. Utility of B-Factors in Protein Science: Interpreting Rigidity, Flexibility, and Internal Motion and Engineering Thermostability. *Chem Rev* **2019**, *119*, 1626-1665, <https://doi.org/10.1021/acs.chemrev.8b00290>.
3. Li, J.; Zhang, H.; Liu, N.; Ma, Y.B.; Wang, W.B.; Li, Q.M.; Su, J.G. Identification of the Intrinsic Motions and Related Key Residues Responsible for the Twofold Channel Opening of Poliovirus Capsid by Using an Elastic Network Model Combined with an Internal Coordinate. *ACS omega* **2023**, *8*, 782-790, <https://doi.org/10.1021/acsomega.2c06114>.
4. Martin, J.N.; Criss, A.K.; Columbus, L. Molecular Determinants of Neisserial Opa Protein Interactions with Human CEACAMs. *Biophysical Journal* **2019**, *116*, 346A-347A, <http://doi.org/10.1016/j.bpj.2018.11.1888>.
5. Sabino, C.P.; Wainwright, M.; Ribeiro, M.S.; Sellera, F.P.; Dos Anjos, C.; da Silva Baptista, M.; Lincopan, N. Global priority multidrug-resistant pathogens do not resist photodynamic therapy. *J Photochem Photobiol B Biol* **2020**, *208*, 111893, <https://doi.org/10.1016/j.jphotobiol.2020.111893>.
6. Azam, M.W.; Khan, A.U. Updates on the pathogenicity status of *Pseudomonas aeruginosa*. *Drug Discov Today* **2019**, *24*, 350-359, <https://doi.org/10.1016/j.drudis.2018.07.003>.
7. Coriolano, D.de L.; de Souza, J.B.; Bueno, E.V.; Medeiros, S.M. de F.R. dos S.; Cavalcanti, I.D.L.; Cavalcanti, I.M.F. Antibacterial and antibiofilm potential of silver nanoparticles against antibiotic-sensitive and multidrug-resistant *Pseudomonas aeruginosa* strains. *Braz J Microbiol* **2021**, *52*, 267-278, <https://doi.org/10.1007/s42770-020-00406-x>.
8. da Silva, D.P.; Matwichuk, M.L.; Townsend, D.O.; Reichhardt, C.; Lamba, D.; Wozniak, D.J.; Parsek, M.R. The *Pseudomonas aeruginosa* lectin LecB binds to the exopolysaccharide Psl and stabilizes the biofilm matrix. *Nat Commun* **2019**, *10*, 2183, <https://doi.org/10.1038/s41467-019-10201-4>.
9. Kasahara, K.; Terazawa, H.; Itaya, H.; Goto, S.; Nakamura, H.; Takahashi, T.; Higo, J. myPresto/omegagene 2020: a molecular dynamics simulation engine for virtual system coupled sampling. *Biophys Physicobiol* **2020**, *17*, 140-146, <https://doi.org/10.2142/biophysico.BSJ-2020013>.
10. Fleming, P.J.; Fleming, K.G. HullRad: Fast Calculations of Folded and Disordered Protein and Nucleic Acid Hydrodynamic Properties. *Biophys J* **2018**, *114*, 856-869. <https://doi.org/10.1016/j.bpj.2018.01.002>.
11. Tiwari, S.P.; Fuglebakk, E.; Hollup, S.M.; Skjærven, L.; Cragolini, T.; Grindhaug, S.H.; Tekle, K.M.; Reuter, N. WEBnm<sup>®</sup> v2.0: Web server and services for comparing protein flexibility. *BMC Bioinform* **2014**, *15*, 427, <https://doi.org/10.1186/s12859-014-0427-6>.
12. Krüger, D.M.; Ahmed, A.; Gohlke, H. NMSim Web Server: integrated approach for normal mode-based geometric simulations of biologically relevant conformational transitions in proteins. *Nucleic Acids Res* **2012**, *40*, W310-W316, <https://doi.org/10.1093/nar/gks478>.
13. Ponzoni, L.; Polles, G.; Carnevale, V.; Micheletti, C. SPECTRUS: A Dimensionality Reduction Approach for Identifying Dynamical Domains in Protein Complexes from Limited Structural Datasets. *Structure* **2015**, *23*, 1516-1525, <https://doi.org/10.1016/j.str.2015.05.022>.
14. Rausch, A.O.; Freiberger, M.I.; Leonetti, C.O.; Luna, D.M.; Radusky, L.G.; Wolynes, P.G.; Ferreira, D.U.; Parra, R.G. FrustratometerR: an R-package to compute local frustration in protein structures, point mutants and MD simulations. *Bioinform* **2021**, *37*, 3038-3040, <https://doi.org/10.1093/bioinformatics/btab176>.
15. Gautam, V.; Chong, W.L.; Chin, S.P.; Zain, S.M.; Rahman, N.A.; Vao-soongnern, V.; Lee, V.S. Loop dynamics behind the affinity of DARPins towards ERK2: Molecular dynamics simulations (MDs) and elastic network model (ENM). *J Mol Liq* **2019**, *274*, 612-620, <https://doi.org/10.1016/j.molliq.2018.10.157>.
16. Kmiecik, S.; Gront, D.; Kolinski, M.; Wieteska, L.; Dawid, A.E.; Kolinski, A. Coarse-Grained Protein Models and Their Applications. *Chem Rev* **2016**, *116*, 7898-7936, <https://doi.org/10.1021/acs.chemrev.6b00163>.
17. Souza, P.C.T.; Thallmair, S.; Conflitti, P.; Ramírez-Palacios, C.; Alessandri, R.; Raniolo, S.; Limongelli, V.; Marrink, S.J. Protein-ligand binding with the coarse-grained Martini model. *Nat Commun* **2020**, *11*, 3714, <https://doi.org/10.1038/s41467-020-17437-5>.
18. Kuriata, A.; Gierut, A.M.; Oleniecki, T.; Ciemny, M.P.; Kolinski, A.; Kurcinski, M.; Kmiecik, S. CABS-flex 2.0: a web server for fast simulations of flexibility of protein structures. *Nucleic Acids Res.* **2018**, *46*, W338-W343, <https://doi.org/10.1093/nar/gky356>.
19. Kurcinski, M.; Oleniecki, T.; Ciemny, M.P.; Kuriata, A.; Kolinski, A.; Kmiecik, S. CABS-flex standalone: a simulation environment for fast modeling of protein flexibility. *Bioinform* **2019**, *35*, 694-695, <https://doi.org/10.1093/bioinformatics/bty685>.
20. Boffoli, D.; Bellato, F.; Avancini, G.; Gurnani, P.; Yilmaz, G.; Romero, M.; Robertson, S.; Moret, F.; Sandrelli, F.; Caliceti, P.; Salmaso, S.; Cámara, M.; Mantovani, G.; Mastrotto, F. Tobramycin-loaded complexes to prevent and disrupt *Pseudomonas aeruginosa* biofilms. *Drug Deliv Transl Res* **2022**, *12*, 1788-1810, <https://doi.org/10.1007/s13346-021-01085-3>.
21. Kumar, S.; Paliya, B.S.; Singh, B.N. Superior inhibition of virulence and biofilm formation of *Pseudomonas aeruginosa* PAO1 by phyto-synthesized silver nanoparticles through anti-quorum sensing activity. *Microb Pathog* **2022**, *170*, 105678, <https://doi.org/10.1016/j.micpath.2022.105678>.
22. Rather, M.A.; Saha, D.; Bhuyan, S.; Jha, A. N.; Mandal, M. Quorum Quenching: A Drug Discovery Approach Against *Pseudomonas Aeruginosa*. *Microbiol Res* **2022**, *264*, 127173, <https://doi.org/10.1016/j.micres.2022.127173>.

23. Ameri, M.; Alipour, M.; Madihi, M.; Nezafat, N. Identification of intrinsically disordered regions in hub genes of acute myeloid leukemia: A bioinformatics approach. *Biotechnol Appl Biochem* **2022**, *69*, 2304-2322, <https://doi.org/10.1002/bab.2287>.
24. Dokainish, H.M.; Re, S.; Mori, T.; Kobayashi, C.; Jung, J.; Sugita, Y. The inherent flexibility of receptor binding domains in SARS-CoV-2 spike protein. *Elife* **2022**, *11*, e75720, <https://doi.org/10.7554/eLife.75720>.
25. Singh, V.; Dhankhar, P.; Dalal, V.; Tomar, S.; Kumar, P. In-silico functional and structural annotation of hypothetical protein from Klebsiella pneumonia: A potential drug target. *J Mol Graph* **2022**, *116*, 108262, <https://doi.org/10.1016/j.jmgm.2022.108262>.
26. Chen, S.; Zhao, Y.; Liu, S.; Zhang, J.; Assaraf, Y.G.; Cui, W.; Wang, L. Epigenetic enzyme mutations as mediators of anti-cancer drug resistance. *Drug Resist Updat* **2022**, *61*, 100821, <https://doi.org/10.1016/j.drug.2022.100821>.
27. Al-Hosni, R.; Ilkan, Z.; Agostinelli, E.; Tammaro, P. The pharmacology of the TMEM16A channel: therapeutic opportunities. *TIPS* **2022**, *43*, 712-725, <https://doi.org/10.1016/j.tips.2022.06.006>.
28. Biswal, M.; Lu, J.; Song, J. SARS-CoV-2 Nucleocapsid Protein Targets a Conserved Surface Groove of the NTF2-like Domain of G3BP1. *J Mol Biol* **2022**, *434*, 167516, <https://doi.org/10.1016/j.jmb.2022.167516>.
29. Gosavi, P.M.; Ngan, K.C.; Yeo, M.J.; Su, C.; Li, J.; Lue, N.Z.; Hoenig, S.M.; Liao, B.B. Profiling the Landscape of Drug Resistance Mutations in Neosubstrates to Molecular Glue Degradors. *ACS Cent Sci* **2022**, *8*, 417-429, <https://doi.org/10.1021/acscentsci.1c01603>.
30. Tomar, P.P.S.; Krugliak, M.; Singh, A.; Arkin, I.T. Zika M—A Potential Viroporin: Mutational Study and Drug Repurposing. *Biomed* **2022**, *10*, 641, <https://doi.org/10.3390/biomedicines10030641>.
31. Nussinov, R.; Zhang, M.; Maloney, R.; Liu, Y.; Tsai, C.J.; Jang, H. Allosteric Cancer Drivers and Innovative Allosteric Drugs. *J. Mol. Biol* **2022**, *434*, 167569, <https://doi.org/10.1016/j.jmb.2022.167569>.
32. Leung, A.K.L.; Griffin, D.E.; Bosch, J.; Fehr, A.R. The Conserved Macrodome Is a Potential Therapeutic Target for Coronaviruses and Alphaviruses. *Pathogens* **2022**, *11*, 94, <https://doi.org/10.3390/pathogens11010094>.
33. Diniz, F.; Coelho, P.; Duarte, H.O.; Sarmiento, B.; Reis, C.A.; Gomes, J. Glycans as Targets for Drug Delivery in Cancer. *Cancers* **2022**, *14*, 911, <https://doi.org/10.3390/cancers14040911>.
34. Xia, Y.; Jayathilake, P.G.; Li, B.; Zuliani, P.; Deehan, D.; Longyear, J.; Stoodley, P.; Chen, J. Coupled CFD-DEM modeling to predict how EPS affects bacterial biofilm deformation, recovery and detachment under flow conditions. *Biotechnol Bioeng* **2022**, *119*, 2551-2563, <https://doi.org/10.1002/bit.28146>.
35. Zhao, Z.; Wang, L.; Miao, J.; Zhang, Z.; Ruan, J.; Xu, L.; Guo, H.; Zhang, M.; Qiao, W. Regulation of the formation and structure of biofilms by quorum sensing signal molecules packaged in outer membrane vesicles. *Sci Total Environ* **2022**, *806*, 151403, <https://doi.org/10.1016/j.scitotenv.2021.151403>.
36. Mechmechani, S.; Gharsallaoui, A.; Karam, L.; EL Omari, K.; Fadel, A.; Hamze, M.; Chihib, N.E. Pepsin and Trypsin Treatment Combined with Carvacrol: An Efficient Strategy to Fight Pseudomonas aeruginosa and Enterococcus faecalis Biofilms. *Microorganisms* **2023**, *11*, 143, <https://doi.org/10.3390/microorganisms11010143>.
37. Tao, J.; Yan, S.; Wang, H.; Zhao, L.; Zhu, H.; Wen, Z. Antimicrobial and antibiofilm effects of total flavonoids from Potentilla kleiniana Wight et Arn on Pseudomonas aeruginosa and its potential application to stainless steel surfaces. *LWT* **2022**, *154*, 112631, <https://doi.org/10.1016/j.lwt.2021.112631>.
38. Gharpure, S.; Yadwade, R.; Chakraborty, B.; Makar, R.; Chavhan, P.; Kamble, S.; Pawar, P.; Ankamwar, B. Bioactive properties of ZnO nanoparticles synthesized using Cocos nucifera leaves. *3 Biotech* **2022**, *12*, 45, <https://doi.org/10.1007/s13205-022-03110-9>.
39. Stoner, S.N.; Baty, J.J.; Scofield, J.A. Pseudomonas aeruginosa polysaccharide Psl supports airway microbial community development. *ISME J* **2022**, *16*, 1730-1739, <https://doi.org/10.1038/s41396-022-01221-y>.
40. Anju, V.T.; Busi, S.; Mohan, M.S.; Ranganathan, S.; Ampasala, D.R.; Kumavath, R.; Dyavaiah, M. In vivo, in vitro and molecular docking studies reveal the anti-virulence property of hispidulin against Pseudomonas aeruginosa through the modulation of quorum sensing. *Int biodeterior biodegrad* **2022**, *174*, 105487, <https://doi.org/10.1016/j.ibiod.2022.105487>.
41. Gheorghita, A.A.; Li, Y.E.; Kitova, E.N.; Bui, D.T.; Pfoh, R.; Low, K.E.; Whitfield, G.B.; Walvoort, M.T.C.; Zhang, Q.; Codée, J.D.C.; Klassen, J.S.; Howell, P.L. Structure of the AlgKX modification and secretion complex required for alginate production and biofilm attachment in Pseudomonas aeruginosa. *Nat Commun* **2022**, *13*, 7631, <https://doi.org/10.1038/s41467-022-35131-6>.
42. Anju, V.T.; Busi, S.; Kumar, S.; Suchiang, K.; Kumavath, R.; Ranganathan, S.; Ampasala, D.R.; Dyavaiah, M. Alantolactone modulates the production of quorum sensing mediated virulence factors and biofilm formation in Pseudomonas aeruginosa. *Biofouling* **2022**, *38*, 331-347, <https://doi.org/10.1080/08927014.2022.2064747>.
43. Jacobs, H.M.; O'Neal, L.; Lopatto, E.; Wozniak, D.J.; Bjarnsholt, T.; Parsek, M.R. Mucoicid Pseudomonas aeruginosa Can Produce Calcium-Gelled Biofilms Independent of the Matrix Components Psl and CdrA. *J Bacteriol* **2022**, *204*, e00568-21, <https://doi.org/10.1128/jb.00568-21>.

44. Hills, O.J.; Yong, C.W.; Scott, A.J.; Devine, D.A.; Smith, J.; Chappell, H.F. Atomic-scale interactions between quorum sensing autoinducer molecules and the mucoid *P. aeruginosa* exopolysaccharide matrix. *Sci Rep* **2022**, *12*, 7724, <https://doi.org/10.1038/s41598-022-11499-9>.
45. Ma, L.Z.; Wang, D.; Liu, Y.; Zhang, Z.; Wozniak, D.J. Regulation of Biofilm Exopolysaccharide Biosynthesis and Degradation in *Pseudomonas aeruginosa*. *Annu Rev Microbiol* **2022**, *76*, 413-433, <https://doi.org/10.1146/annurev-micro-041320-111355>.
46. Wüllner, D.; Gesper, M.; Haupt, A.; Liang, X.; Zhou, P.; Dietze, P.; Narberhaus, F.; Bandow, J.E. Adaptive Responses of *Pseudomonas aeruginosa* to Treatment with Antibiotics. *Antimicrob Agents Chemother* **2022**, *66*, e00878-21, <https://doi.org/10.1128/AAC.00878-21>.
47. Chadha, J.; Harjai, K.; Chhibber, S. Repurposing phytochemicals as anti-virulent agents to attenuate quorum sensing-regulated virulence factors and biofilm formation in *Pseudomonas aeruginosa*. *Microb Biotechnol* **2022**, *15*, 1695-1718, <https://doi.org/10.1111/1751-7915.13981>.
48. Roque-Borda, C.A.; da Silva, P.B.; Rodrigues, M.C.; Di Filippo, L.D.; Duarte, J.L.; Chorilli, M.; Vicente, E.F.; Garrido, S.S.; Pavan, F.R. Pharmaceutical nanotechnology: Antimicrobial peptides as potential new drugs against WHO list of critical, high, and medium priority bacteria. *Eur J Med Chem* **2022**, *241*, 114640, <https://doi.org/10.1016/j.ejmech.2022.114640>.
49. Nabi, M.; Zargar, M.I.; Tabassum, N.; Ganai, B.A.; Wani, S.U.D.; Alshehri, S.; Alam, P.; Shakeel, F. Phytochemical Profiling and Antibacterial Activity of Methanol Leaf Extract of *Skimmia anquetilia*. *Plants* **2022**, *11*, 1667, <https://doi.org/10.3390/plants11131667>.